Breaking the causality limit for broadband acoustic absorption using a noncausal active absorber
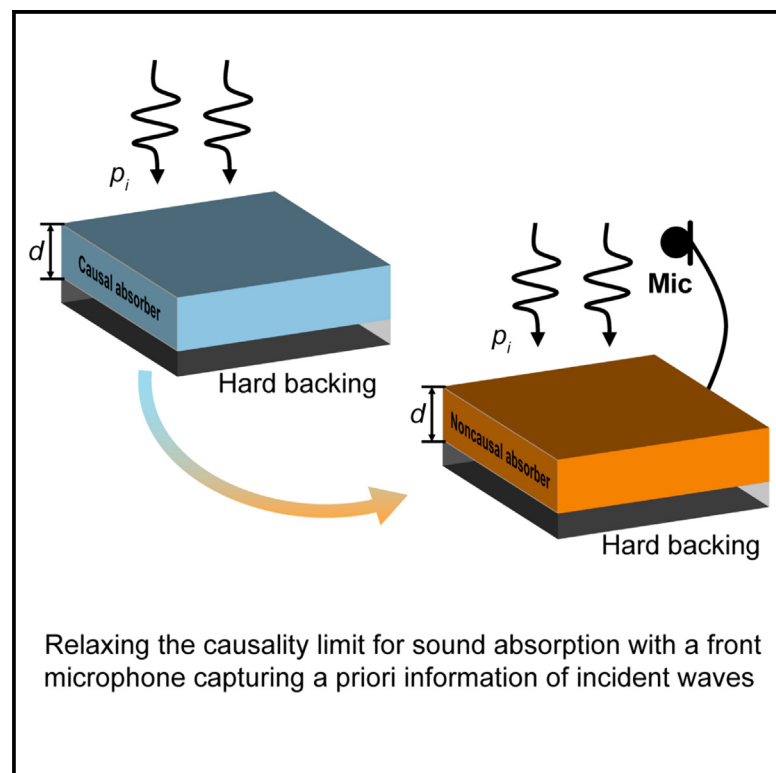
Graphical abstract

Relaxing the causality limit for sound absorption with a front microphone capturing a priori information of incident waves

Authors

Kangkang Wang, Sipei Zhao, Chen Shen, Li Shi, Haishan Zou, Jing Lu, Andrea Alù

Correspondence

shenc@rowan.edu (C.S.),
lujing@nju.edu.cn (J.L.),
aalu@gc.cuny.edu (A.A.)

In brief

The causality constraint on the thickness and bandwidth of acoustic absorbers can be overcome by leveraging *a priori* information of the incident waves. An updated physical limit between the thickness and absorption bandwidth is derived for noncausal absorbers. A noncausal sound absorber is designed with enhanced absorption performance. The absorber can be tuned through the control network that feeds the information on the incoming signals, achieving adjustable absorption spectra without the need for structural modifications.

Highlights

- The causality limit for sound absorption can be overcome by sampling incident signals

- The trade-off between causality violation, bandwidth, and thickness was derived

- An active sound absorber was demonstrated with performance beyond the causality limit

- Tunable absorption features of the designed active absorber were presented
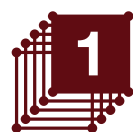
Understand

Early stage research on device properties, design, and physics

 CellPress

Article

Breaking the causality limit for broadband acoustic absorption using a noncausal active absorber

Kangkang Wang,[1,6] Sipei Zhao,[2,6] Chen Shen,[3,*] Li Shi,[1] Haishan Zou,[1] Jing Lu,[1,*] and Andrea Alù[4,5,7,*]

[1]Key Laboratory of Modern Acoustics, MOE, Institute of Acoustics, Department of Physics, Nanjing University, Nanjing 210093, P.R. China
[2]Centre for Audio, Acoustics and Vibration, Faculty of Engineering and IT, University of Technology Sydney, Ultimo, NSW 2007, Australia
[3]Department of Mechanical Engineering, Rowan University, Glassboro, NJ 08028, USA
[4]Photonics Initiative, Advanced Science Research Center, City University of New York, New York, NY 10031, USA
[5]Physics Program, Graduate Center, City University of New York, New York, NY 10016, USA
[6]These authors contributed equally
[7]Lead contact
*Correspondence: shenc@rowan.edu (C.S.), lujing@nju.edu.cn (J.L.), aalu@gc.cuny.edu (A.A.)
https://doi.org/10.1016/j.device.2024.100502

THE BIGGER PICTURE   Broadband absorption in thin films is of fundamental importance for several physics and engineering applications. However, the principle of causality—i.e., the fact that the response of a system is only influenced by past excitations—imposes a trade-off between the thickness and bandwidth of absorbers. To overcome this constraint, we introduce an active platform that provides *a priori* information to the absorber by sampling the incoming signal ahead of time, realizing a noncausal response. We derived a general relation between the minimum thickness of an absorber, its bandwidth, and the degree of causality violation. Unlike active noise cancellation like that found in modern headphones, which operate based on the generation of interference signals with similar intensity to the source, a noncausal absorber has much lower power requirements. To demonstrate this concept, we created a sub-wavelength active absorber that overcomes the causality limitation, showcasing a large absorption bandwidth beyond the conventional limit.

SUMMARY

The principle of causality imposes a constraint between the thickness and bandwidth of absorbers. This trade-off applies to any linear, time-invariant, passive system, limiting the development of broadband-absorbing materials that demand a thin profile for sound, light, and radio waves. Here, we demonstrate a strategy to overcome this constraint in acoustics using a noncausal active absorber whose response is controlled over time. A theoretical framework is established, which sets a relation among minimum thickness, bandwidth, and *a priori* information about the incident signal, representing a relaxed physical bound for noncausal absorbers. We design an absorber based on this principle and experimentally show that its response bandwidth surpasses the conventional limit. Our results showcase an active metamaterial that reduces the footprint of acoustic absorbers and elucidate the role of prior information in enhancing acoustic technologies, offering insights into the design of active acoustic devices.

INTRODUCTION

Causality requires the material response to an incoming wave at any given moment to be solely determined by the input information before that moment. This places stringent constraints on the response of linear, time-invariant media, which are manifested as various practical limits, e.g., the general constraints on the frequency response and dispersion of materials described by Kramers-Kronig relations,[1,2] the limit on the bandwidth of small radiators and antennas known as Chu's limit,[3–6] the Bode-

Fano limit on the matching bandwidth of reactive loads,[7–9] limits on the cloaking bandwidth of metamaterials,[10–13] and the dispersion constraints on acoustic Willis coupling.[14,15] Another manifestation of causality in wave phenomena is the fundamental trade-off between the thickness and bandwidth of wave absorbers, as first demonstrated by Rozanov in the field of electromagnetic waves[16] and later extended to acoustics.[17,18] This absorption limit is a universal constraint applicable to all passive, causal, linear, and time-invariant absorbers. It represents an important trade-off in developing broadband absorbers,

implying that perfect absorption can only be achieved at a single frequency[19–21] and a minimum thickness requirement arises to achieve near-unity absorption across a given bandwidth.[18,22] Recently, research efforts have been devoted to approaching this causality limit for absorbers, and several strategies have been proposed to get close to it, such as combining different resonant units to achieve broadband, near-optimal absorbers.[18,22–24] However, their causal nature implies a trade-off between their thickness and the absorption performance, a restriction that becomes particularly pronounced when tackling broadband low-frequency noise.

A few methods have been proposed to overcome this limit, circumventing different underlying assumptions. For example, by replacing the hard boundary backing of the absorber with a soft boundary, near-total sound absorption within the 50–200 Hz range has been achieved using a 0.5-cm-thick metallic mesh absorber, lower than the minimum thickness set forth by the hard boundary counterpart.[25] By switching to a soft boundary backing, the thickness limit pivots on the static density rather than the bulk modulus of the material and can easily be circumvented by employing a high-density material. However, a broadband soft boundary backing is difficult to realize, especially in air because of its low characteristic impedance. Time-varying absorbers[9,26–33] have also been explored as a platform to overcome Rozanov's bound. They can achieve superior absorption or scattering properties based on switched operations[30–33] that break the assumption of time invariance underlying the bound. Nonetheless, these methods are often limited to specific temporal forms of excitation and cannot be generalized to arbitrary excitation schemes. Continuous periodic time modulation may present an avenue for developing broadband absorbers capable of handling arbitrary waveforms.[9] Active approaches can also overcome the causality bound, offering versatility in wave manipulation and their interaction with matter. Compared to passive systems, active materials can amplify the impinging waves and induce strong responses, enhancing their tunability and reconfigurability.[34] Various strategies have been proposed to realize active metamaterials, e.g., to realize parity-time-symmetric[35,36] and nonreciprocal[37,38] responses. Using non-Foster circuit elements is a common strategy to broaden the bandwidth using active modular components,[6,39,40] but they pose challenges associated with instability and noise. Yet, absorbers designed using such active elements suggest that they can lead to superior performance in terms of absorption.[40]

In this work, we establish a theoretical framework for acoustic absorbers that are generally noncausal and present a design for an absorber that breaks causality by introducing active elements. We start by establishing a relationship between the minimum thickness of absorbers and the degree of causality violation, which defines the physical limits for noncausal active absorbers (NCAAs). Subsequently, we design and experimentally implement an NCAA with a near-perfect absorption within the 150–1,600 Hz frequency range, boasting an average absorption of 98%, far surpassing the performance of conventional passive absorbers of the same thickness. Our approach achieves a noncausal response by employing an active unit that leverages *a priori* information on the incident signal. This enables the designed absorber to utilize not only the incident wave information

at the current and preceding moments but also its evolution in the future, which breaks causality. The proposed NCAA is 82.5 mm thick, much thinner than the equivalent minimum thickness of 374.3 mm determined by the causality limit for the achieved bandwidth of operation.

RESULTS

Theory of surpassing Rozanov limit with noncausal responses

Conventional sound-absorbing materials are expected to adhere to causality,[41] which imposes constraints on their interaction with acoustic waves. Consider the case of acoustic wave propagation in air, where a homogeneous sound-absorbing material of thickness d is placed on a hard boundary backing, as in Figure 1A. In this case, when an acoustic beam p_i is incident on the absorbing material, causality implies that the reflected wave $p_r(t)$ at any given moment t is determined solely by the incident signal before that moment. Consequently, the reflection coefficient $R(\omega)$ is an analytic function of complex ω in the upper half of the complex ω plane. Leveraging the analytical nature of $R(\omega)$, an inequality between the absorption coefficient $A(\lambda) = 1 - |R(\lambda)|^2$ and the material thickness d can be derived:[18]

$$d_{\min} = \frac{B_{\text{eff}}}{4\pi^2 B_0}\left|\int_0^\infty \ln[1 - A(\lambda)]d\lambda\right| \leq d, \qquad \text{(Equation 1)}$$

where λ is the sound wavelength in air, B_0 is the bulk modulus of air, and B_{eff} is the effective bulk modulus of the absorber in the static limit ($|\lambda| \rightarrow \infty$). The equation yields a fundamental limitation of the thickness of any passive absorber with a prescribed absorption characteristic, and hence a trade-off is found between the absorption performance (i.e., the absorption coefficient and bandwidth) and the material thickness. This limit is denoted as the causality limit in the subsequent discussions. One may assume that an ideal absorber to achieve a specific absorption spectrum within the frequency band $[f_0, \infty]$, as shown in Figure 1C. By taking the absorption spectrum from Figure 1C into the integral equation on the left-hand side of Equation 1, we obtain the required thickness d of the absorber as a function of f_0 in Figure 1D. It is evident that as the frequency f_0 decreases (i.e., a broader bandwidth), the required thickness of the absorber rapidly increases. This phenomenon arises due to the growth of the wavelength for lower frequencies, exerting a greater impact on the absorber thickness. Therefore, broadband low-frequency sound absorption demands a substantial thickness.[42] This fundamental challenge underscores the difficulty in handling low-frequency broadband noise with conventional sound-absorbing materials.

To achieve broadband sound absorption at low frequencies using ultra-thin acoustic materials, we turn our attention to active absorbers that overcome Equation 1 by breaking one of the underlying assumptions in its derivation: the principle of causality. A noncausal absorber, as the name suggests, overcomes causality because its response, e.g., the reflected wave $p_r(t)$, at any given moment t is no longer solely determined by the incident wave information that has already reached the
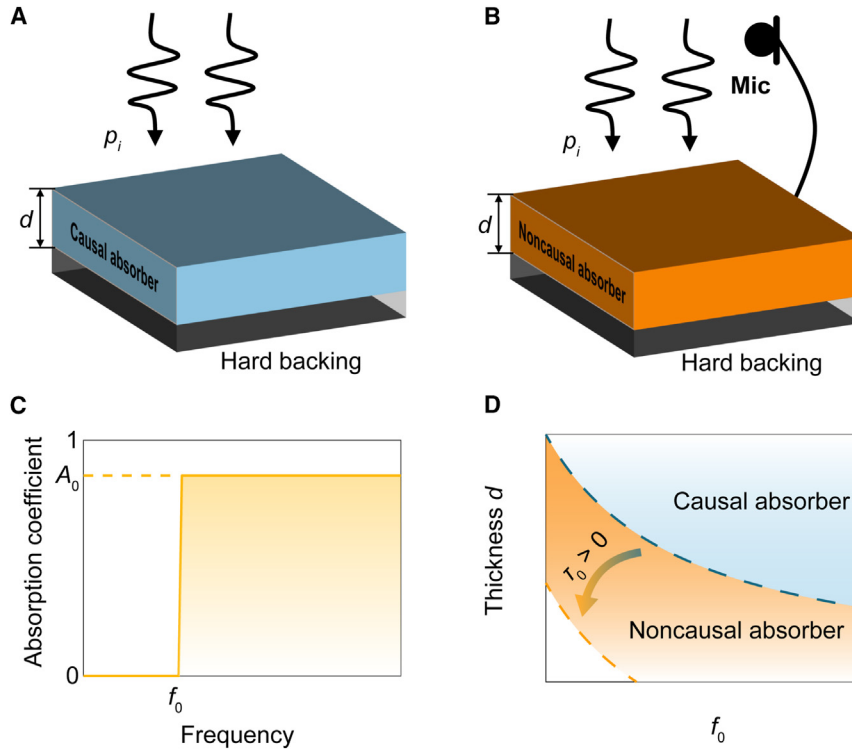
Figure 1. Comparison of causal and noncausal absorbers

(A) A causal absorber of thickness d backed by a hard boundary.

(B) A noncausal absorber of thickness d backed by a hard boundary, with a front microphone capturing *a priori* information of the incident wave before reaching the absorber.

(C) The desired absorption spectrum with a large absorption coefficient A_0 within the frequency band $[f_0, \infty]$.

(D) Schematic diagram of the required absorber thickness d versus f_0 to achieve the absorption spectrum in (C). By introducing a noncausal material responding for $\tau_0 > 0$, the causal limit (cyan dashed line) is lifted, and a more relaxed noncausal limit (saffron dashed line) applies. A noncausal absorber achieves sound absorption equivalent to a much thicker causal absorber.

absorber but is also influenced by *a priori* information on the incoming wave profile before it actually arrives. This feature is not possible with passive systems, but it can be enabled, for instance, by a front microphone that transmits the incident wave information to the noncausal absorber before it reaches the absorber itself (Figure 1B). This makes the absorber leverage the incident wave information from the future. This is the key to break the causality limit, as it will be shown in the following derivation. Since the noncausal absorber still satisfies linearity and time invariance, its interaction with the incident acoustic wave p_i can be described by a concise convolution relation

$$p_r(t) = \int_{-\tau_0}^{\infty} r'(\tau)p_i(t - \tau)d\tau \qquad \text{(Equation 2)}$$

where $r'(\tau)$ denotes the response kernel of the incident wave interaction with the noncausal absorber, which satisfies $r'(\tau) = 0$ for $\tau < -\tau_0$ (τ_0 is a positive real number), while $r'(\tau) \neq 0$ for $\tau \geq -\tau_0$. Here, τ_0 denotes the introduced noncausal component, and a larger τ_0 is associated with a larger degree of causality breaking. The nonzero response with respect to the incoming wave in the future ($\tau < 0$) clearly indicates a noncausal response process. Assuming that the system remains linear, and by carrying out the Fourier transform of Equation 2 (with harmonic time factor $e^{i\omega t}$), the reflection coefficient $R(\omega)$ in the frequency domain may be obtained as

$$R(\omega) = \frac{p_r(\omega)}{p_i(\omega)} = \int_{-\tau_0}^{\infty} r'(\tau)e^{i\omega\tau}d\tau. \qquad \text{(Equation 3)}$$

Equation 3 reveals that the presence of noncausal components in the reflection coefficient $R(\omega)$ makes it nonanalytic in the upper half of the complex ω plane, distinct from the case of causal absorbers.[18] However, by multiplying $e^{i\omega\tau_0}$ on both sides of Equation 3, $R(\omega) e^{i\omega\tau_0}$ is analytic in the upper half of the complex ω plane. As a result, we can establish the following inequality for the absorption coefficient $A(\lambda)$ of noncausal absorbers:

$$d_{\min} = \frac{B_{\text{eff}}}{4\pi^2 B_0}\left|\int_0^{\infty} \ln[1 - A(\lambda)]d\lambda\right| \leq d + \frac{B_{\text{eff}}c_0}{2B_0}\tau_0,$$

$$\text{(Equation 4)}$$

where c_0 is the speed of sound in air. A detailed derivation of Equation 4 is presented in Note S1. It is evident that for a noncausal absorber with $\tau_0 > 0$, the original causality constraint is relaxed. Remarkably, the term ($B_{\text{eff}} c_0\tau_0/2B_0$) on the right-hand side of Equation 4 increases linearly as τ_0 grows, leading to a decrease in the minimum thickness requirement for noncausal absorbers. This implies that, for an equivalent absorption performance, the thickness of a noncausal absorber can be reduced compared to the one of a conventional causal absorber, as visualized in Figure 1D. When no noncausal component is introduced ($\tau_0 = 0$), Equation 4 becomes the same as Equation 1, as expected. Furthermore, Equation 4 implies the existence of an upper limit to the sound absorption performance of the noncausal absorber, determined by the actual absorber thickness d and the introduced noncausal component τ_0.

Design of the NCAA

The designed active absorber is shown in Figure 2A. The main body of the absorber is marked in the red dashed box, with thickness d, and realized by the loudspeaker embedded in air, mainly containing the loudspeaker and the cavity between
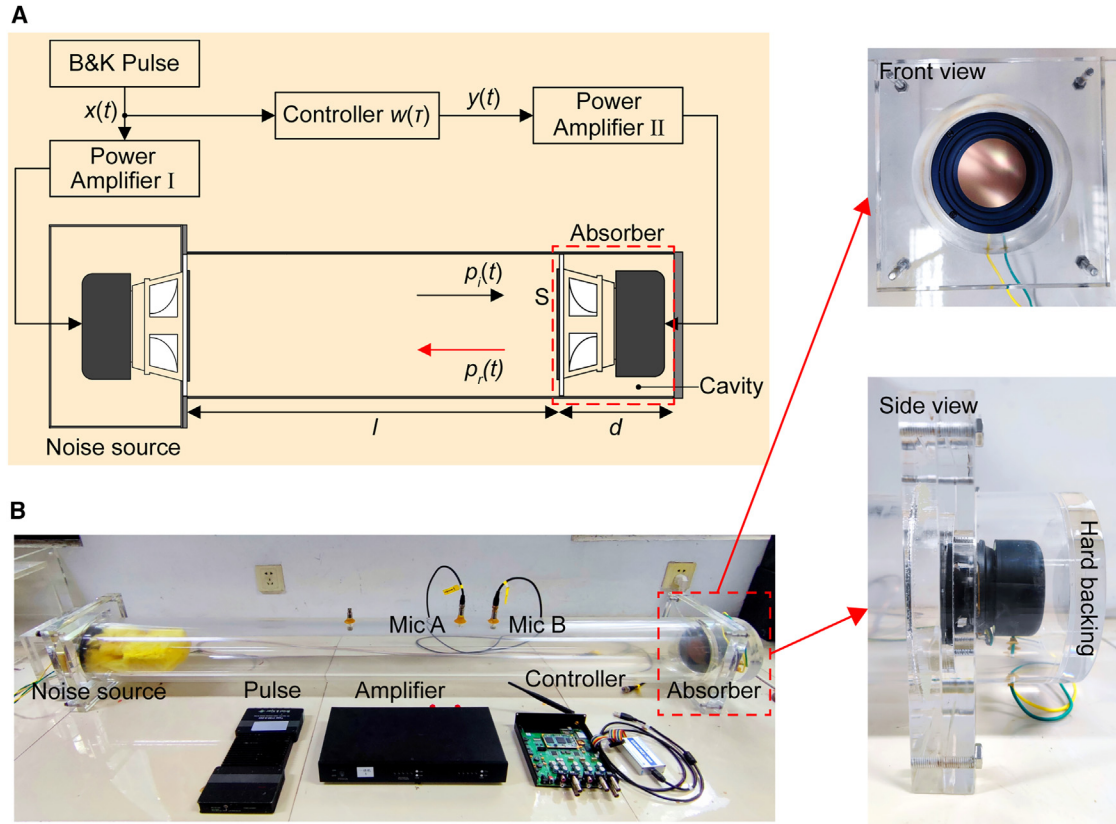
Figure 2. Design of the NCAA

(A) Schematic diagram of the designed active absorber. The absorber with thickness d is highlighted by the red dashed box, whose main body comprises two components: the loudspeaker and the cavity.

(B) Photograph of the experimental system. The two subplots show the front and side views of the absorber, respectively.

the loudspeaker and the hard boundary backing. A noise source is positioned at the left end of the waveguide, separated by a distance l from the active absorber. The noise signal $x(t)$, generated by a multichannel analyzer (B&K PULSE 3160A) and amplified by a power amplifier I, is utilized to stimulate a plane wave that impinges upon the absorber. We label the incident wave $p_i(t)$ and the reflected wave $p_r(t)$ at the interface S of the absorber at time t. To achieve efficient sound absorption, it is crucial to control the absorber to generate an anti-reflection signal that can induce destructive interference with the reflected wave after the incident wave $p_i(t)$ interacts with the absorber, thus leading to perfect absorption. Therefore, for the sake of understanding, the reflected wave $p_r(t)$ at the interface S of the active absorber can be considered as a superposition of two parts (see Figure 2A). One part is generated by the reflection of the incident wave $p_i(t)$ at the active absorber, which can be regarded as the passive reflected wave, $p_{r_P}(t)$. The other portion is the anti-reflection signal generated by the active absorber, which can be regarded as the active reflected wave, $p_{r_A}(t)$. The overall reflected wave $p_r(t)$ at the interface S of the absorber can be written as the sum of these two components:

$$p_r(t) = \int_0^\infty r_P(\tau)p_i(t-\tau)d\tau + \frac{A_2 S_2}{A_1 S_1}\int_{-\frac{l}{c_0}+t_1}^\infty w\left(\tau + \frac{l}{c_0} - t_1\right)p_i(t-\tau)d\tau,$$

(Equation 5)

where $r_P(\tau)$ is the passive response kernel in the time domain. This response still satisfies the causality condition, i.e., $r_P(\tau) = 0$ when $\tau < 0$. A_1 and A_2 represent the amplification factors of power amplifiers I and II, respectively. S_1 and S_2 denote the sensitivity of the noise source loudspeaker and the loudspeaker in the absorber, respectively. The variable t_1 is the inherent time delay imposed by the hardware components of the controller. $w(\tau)$ is the time-domain response of the controller, which needs to be physically realizable. Hence, it must also be a causal response, i.e., $w(\tau) = 0$ when $\tau < 0$. A detailed derivation of Equation 5 is described in Note S2.

For the sake of simplicity, an ideal noise signal $x(t)$ is used to play the role of the microphone in Figure 1B. In practical applications, a small front microphone or an array of small microphones can be used to capture the *a priori* information necessary to

break causality. Moreover, advanced measurement techniques like laser Doppler vibrometry[43,44] may be employed to obtain the *a priori* information in a remote manner. In the case of this experiment, the noise signal $x(t)$ is equivalent to a "sentry" and serves as a reference signal to provide *a priori* information of the incident wave for the active absorber so that the absorber can obtain the incident wave information before the incident wave reaches the absorber. When $l/c_0 > t_1$, Equation 5 can be simplified as

$$p_r(t) = \int_{-\tau_0}^{\infty} \left(r_P(\tau) + \frac{A_2 S_2}{A_1 S_1} w(\tau + \tau_0) \right) p_i(t - \tau) d\tau, \tag{Equation 6}$$

where $\tau_0 = l/c_0 - t_1$ is the noncausal component introduced by the active absorber. According to Equation 6, the negative lower limit of integration highlights that the reflected wave for the active absorber at time t relies not only on the incident wave information at time t and before but also on information from future portions of the incident signal. This clearly indicates a noncausal response. It follows that the noncausal absorber can be successfully designed with the introduction of the noncausal component τ_0.

On the other hand, when $\tau_0 \leq 0$, we can obtain the relationship between the reflected wave $p_r(t)$ and the incident wave $p_i(t)$ of the active absorber by simplifying Equation 5:

$$p_r(t) = \int_{0}^{\infty} \left(r_P(\tau) + \frac{A_2 S_2}{A_1 S_1} w(\tau + \tau_0) \right) p_i(t - \tau) d\tau. \tag{Equation 7}$$

Evidently, the determination of the reflected wave of the active absorber at time t only relies on the information of the incident wave at time t and before. Hence, the absorber remains causal; however, it is an active system, and its sound absorption performance must adhere to the causal limit as outlined by Equation 1.

The combination of Equations 6 and 7 shows that the active absorber is not necessarily noncausal, and whether it introduces a noncausal component depends mainly on the magnitude of the propagation time l/c_0 of the noise path and the inherent time delay t_1 of the controller. Specifically, when $\tau_0 > 0$, the active absorber exhibits noncausal behavior. Conversely, when $\tau_0 \leq 0$, the active absorber system remains causal. Based on Equation 4, the upper limit of achievable sound absorption performance for the noncausal absorber increases linearly with the introduction of the noncausal component. This implies that intentionally increasing the propagation time l/c_0 of the noise path or decreasing the inherent time delay t_1 of the controller during the design of the NCAA can improve the upper limit of absorption performance. By effectively breaking the causal limit, this approach facilitates the realization of ultra-broadband sound absorption using a compact underlying structure. This guideline holds significant importance for the design of noncausal absorbers and presents a potential solution for the treatment of low-frequency broadband noise.

In order to further investigate the effect of the introduced noncausal component τ_0 on the absorption performance of the

NCAA, a pure time delay t_2 is introduced between the signal $x(t)$ and the controller $w(\tau)$. This time delay can be tuned by programming in the digital signal processor (DSP). Calculations reveal that the noncausal component introduced by the NCAA becomes $\tau_0 = l/c_0 - t_1 - t_2$ at this stage. The noncausal component τ_0 can be adjusted by varying the time delay t_2. Specifically, when $t_2 = 0$, the active noncausal absorber introduces the maximum noncausal component, and as t_2 increases ($t_2 > 0$), the noncausal component τ_0 gradually decreases. After adding the pure time delay t_2, the controller response $w'(\tau)$ can be calculated as

$$w'(\tau) = w(\tau + t_2). \tag{Equation 8}$$

A detailed derivation of Equation 8 is given in Note S3.

Experimental testing of the NCAA

Experiments were conducted in a circular impedance tube (Figure 2B) with a diameter of $d_0 = 12$ cm. The tube wall, made of 20-mm-thick plexiglass, provides sound insulation of over 25 dB above 150 Hz as predicted by the mass law. The noise source and the active absorber were positioned at the two ends of the impedance tube. The separation distance $l = 1.5$ m was chosen to provide space to investigate the absorption performance of the noncausal absorber for different noncausal conditions. To mitigate the impact of multiple reflections within the tube, some glass wool was employed. The active absorber, with a thickness of $d = 82.5$ mm, consists of a loudspeaker embedded in air and backed by a 20-mm-thick plexiglass plate, serving as a hard boundary to prevent sound energy leakage. In the static limit, the active absorber can be treated as a homogeneous material. Its effective bulk modulus could be calculated using Wood's formula[45] $B_{\text{eff}}^{-1} = \phi B_0^{-1} + (1 - \phi) B_{\text{solid}}^{-1}$, where $\phi = V_{\text{air}}/V_{\text{tot}}$ represents the air-filling rate in the material, B_0 is the bulk modulus in air, and B_{solid} is the bulk modulus of the solid component. Since $B_{\text{solid}} \gg B_0$, $B_{\text{eff}} = B_0/\phi$. Notably, the static effective bulk modulus B_{eff} of the active absorber primarily depends on the air filling rate ϕ, which can be estimated by considering the dimensions of the components in the active absorber, yielding an approximate value of $B_{\text{eff}} = 1.3 B_0$.

During the experiments, to ensure that only the plane wave mode is excited, low-pass white noise below 1,600 Hz is emitted from the noise source. The upper limit of the absorption range was constrained by the cutoff frequency of the waveguide, which is 1,657 Hz and could be further increased with a smaller impedance tube. The DSP of the controller is implemented using a TMS320C6748 chip with a sampling rate of $f_s = 16,000$ Hz. The DSP has a built-in time delay of $t_1 = 0.26$ ms and incorporates an embedded finite impulse response filter with an order of $N = 1,023$. The optimal time-domain impulse response of the controller in the experiment, denoted as $\mathbf{w}_{\text{opt}}(n)$ (the discretized form of $w_{\text{opt}}(\tau)$), is obtained by optimizing based on a filtered-reference least mean squares (FXLMS) algorithm.[46] The frequency response of this optimal controller is illustrated in Figures S1C and S1D. Detailed information regarding this optimization algorithm can be found in Note S4.

To quantitatively evaluate the role of causality breaking in sound absorption, the noncausal component τ_0 is varied,
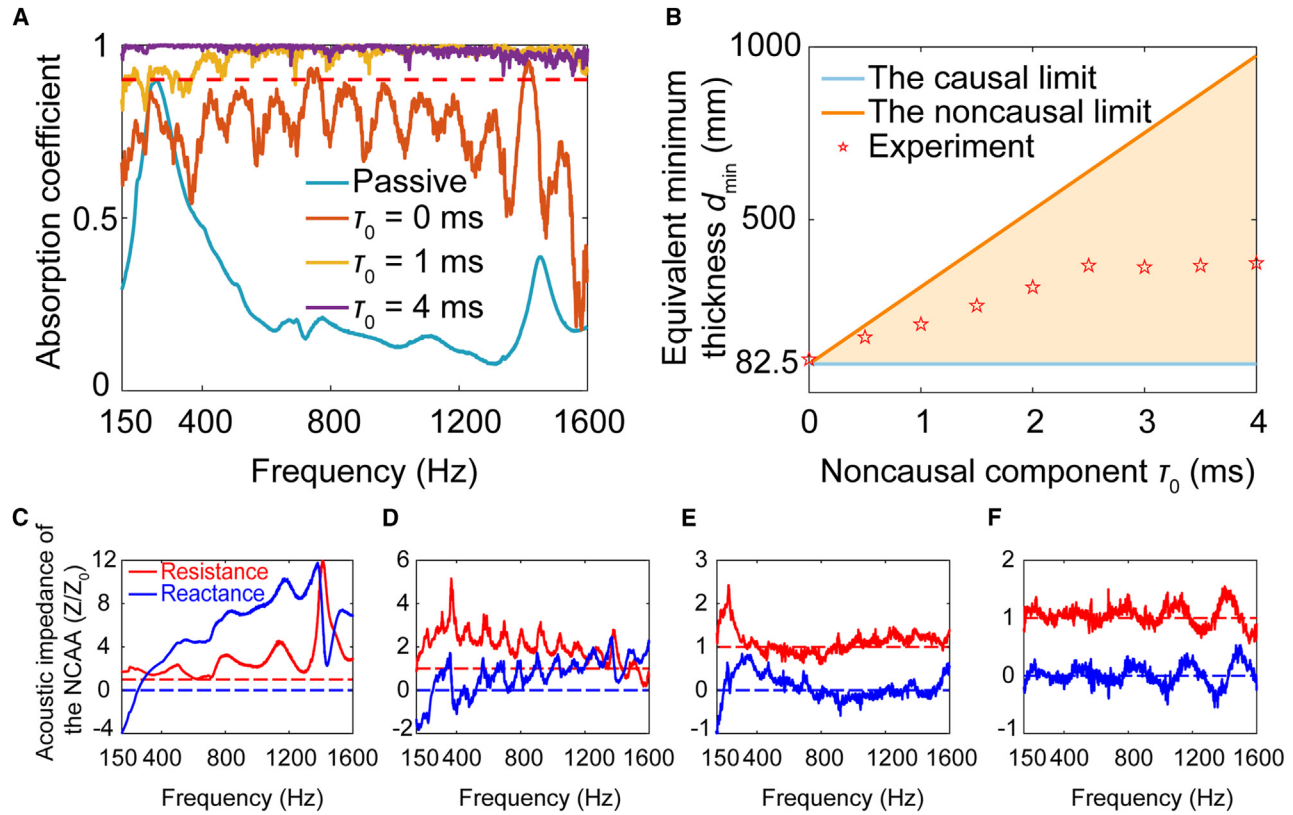
Figure 3. Experimental results of the proposed NCAA

(A) Absorption spectrum of the NCAA for different τ_0 values, namely 0, 1, and 4 ms, compared with the passive absorption. The red dashed line serves as a reference, representing an absorption coefficient of 0.9.

(B) Variation of the equivalent minimum material thickness d_{min} with τ_0 is examined by substituting the absorption spectrum for different τ_0 cases into the left side of Equation 4. The yellow shaded area corresponds to the exceeded absorption performance enabled by the noncausal absorber compared to a causal counterpart of the same thickness.

(C–F) Acoustic impedance Z/Z_0 at the interface S of the NCAA for the passive situation, $\tau_0 = 0$ ms, $\tau_0 = 1$ ms, and $\tau_0 = 4$ ms, corresponding to the four cases in (A), respectively. The impedance can be inferred from the measured reflection coefficient R, i.e., $Z/Z_0 = (1 + R)/(1 - R)$. Z_0 is the characteristic acoustic impedance of the air.

and its impact on the absorption performance is investigated. The discrete form of Equation 8 leads to $\mathbf{w}_{opt}'(n) = \mathbf{w}_{opt}(n + t_2 \cdot f_s)$ during the experiments, where $\mathbf{w}_{opt}'(n)$ represents the optimal controller response after incorporating the time delay t_2. By advancing $t_2 \cdot f_s$ sampling points, the controller response $\mathbf{w}_{opt}'(n)$ with the addition of the time delay t_2 can be obtained from the optimal controller $\mathbf{w}_{opt}(n)$ at $t_2 = 0$. Therefore, the absorption coefficients corresponding to different noncausal components τ_0 can be determined. Three typical examples are shown in Figure 3A for different τ_0 as 0, 1, and 4 ms, respectively, compared with the passive absorption. Interestingly, even in the absence of active control, the absorber still exhibits a remarkable absorption performance approaching 0.9 at 260 Hz. However, this performance is achieved with a narrow bandwidth. This outcome can be attributed to the fact that the loudspeaker is a second-order resonant system, behaving as a passive Helmholtz resonator capable of strong absorption but with a narrow linewidth. Taking the absorption spectrum at this point into the integral equation on the left-hand side of Equation 1 yields $d_{min} = 56.3$ mm $< d =$ 82.5 mm. This confirms that the thickness of the absorber still falls within the causal limit as expected since no active control function is used. Once the active control of the absorber is turned on, the absorption performance will start improving. By increasing the noncausal component to 4 ms, the NCAA achieves absorption greater than 0.9 across the entire frequency band of interest, 150–1,600 Hz, with a remarkably flat absorption spectrum. Based on the absorption spectrum measured at different noncausal components τ_0, the left-hand side of Equation 4 is evaluated to yield the equivalent minimum material thickness d_{min} shown in Figure 3B. The figure demonstrates that introducing a noncausal component $\tau_0 > 0$ enables the absorber to exceed the causal limit, with the degree of causality breaking manifested by the gradual increase of d_{min} with larger τ_0 values, e.g., when $\tau_0 = 4$ ms, the equivalent minimum material thickness reaches 374.3 mm. This value surpasses the actual thickness $d = 82.5$ mm of the absorber, representing a more than 4-fold thickness reduction by adopting the active system. At $\tau_0 = 0$ ms, which represents that the absorber is causal, the calculated
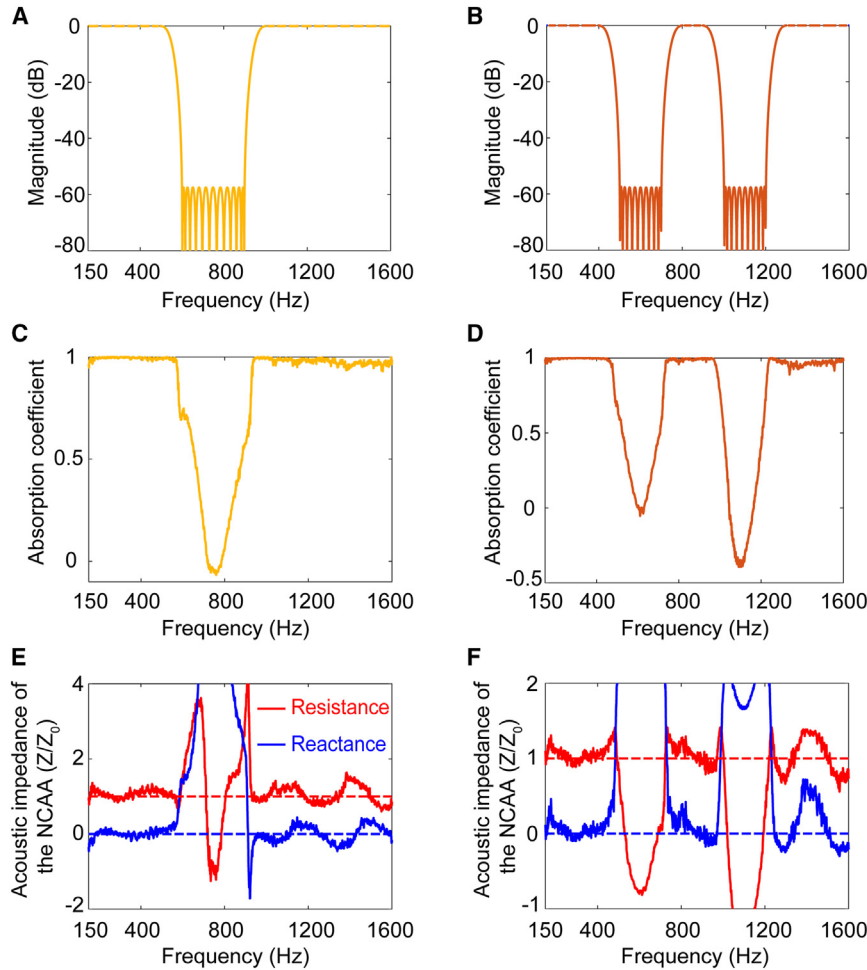
CellPress
OPEN ACCESS

Figure 4. Programmable absorption spectrum by the NCAA

(A and B) The shaping filters $f_1(n)$ and $f_2(n)$ are shown in (A) and (B), respectively.

(C and D) The absorption spectrum of the NCAA with the shaping filters $f_1(n)$ and $f_2(n)$ is illustrated in (C) and (D) respectively.

(E and F) The acoustic impedance Z/Z_0 at the interface S of the NCAA corresponds to the absorption spectrum in (C) and (D), respectively.

controller without physically altering the structure, offering unparalleled flexibility and tunability.

For the NCAA, the filtered-E least mean squares (FELMS) optimization algorithm[48] based on a shaping filter can be used to achieve a tunable sound absorption spectrum. The core of the algorithm is based on the FXLMS algorithm by adding a shaping filter $f(n)$ to filter the error signal $e(n)$, which is equivalent to the reflected wave p_r (see Note S4), and then updating the controller $\mathbf{w}(n)$ to achieve a constraint on the absorption spectrum (see Note S5). As shown in Figures 4A and 4B, two representative shaping filters are designed. Specifically, Figure 4A corresponds to a single stopband filter, denoted as $f_1(n)$, with the stopband frequency range of 600–900 Hz. Using $f_1(n)$ to filter the error signal $e(n)$ means that the 600–900 Hz frequency band does not need to be cancelled, i.e., the sound waves within this band are reflected. Figure 4B represents a double stopband filter, referred to as $f_2(n)$, with stopband frequency ranges of 500–700 and 1,000–1,200 Hz, respectively. Following the application of the shaping filters $f_1(n)$ and $f_2(n)$ to filter the error signal $e(n)$, the optimal controllers are obtained based on the FELMS algorithm, with the resulting absorption spectrums presented in Figures 4C and 4D, respectively. In Figure 4C, the average absorption coefficient of the NCAA within the 600–900 Hz frequency band is merely 0.28, while the other bands remain nearly unaffected, exhibiting an average absorption coefficient of 0.97 in the near-unitary absorption. Following the absorption spectrum, the right-hand side of Equation 4 is calculated to be d_{min} = 339.2 mm, still exceeding the actual thickness of 82.5 mm of the NCAA, and is unattainable by causal absorbers. Similarly, in Figure 4D, the absorption coefficient of the NCAA within the double stop bands of 500–700 and 1,000–1,200 Hz is also remarkably low, averaging only 0.11. In contrast, the absorption coefficient in the other frequency bands remains considerably high. Utilizing the absorption spectrum within the integral equation on the left side of Equation 4 yields d_{min} = 334.9 mm, which, once again, surpasses the thickness of the NCAA. The substantial variation in the absorption coefficient between the stopband and the passband stems from the rapid

minimum thickness is d_{min} = 95.9 mm and slightly exceeds the actual absorber thickness of 82.5 mm. The small discrepancy may be caused by measurement errors or a small amount of sound energy leakage. Clearly, continuing to increase the noncausal component is beneficial to elevate the absorption performance of the NCAA. This phenomenon can be attributed to the continuously improved impedance matching shown in Figures 3C–3F, which is calculated corresponding to the four cases in Figure 3A.

Broadband absorber with tunable absorption features

To highlight the versatility of the proposed NCAA in programmable sound absorption, we vary the optimization algorithm to achieve selective reflection in tunable frequency bands while ensuring high absorption in other bands. This feature finds practical utility in scenarios where a specific acoustic frequency band needs to be reflected more prominently, for example, in selective sound communication. While passive metamaterial absorbers can, in principle, achieve similar functionality by adjusting the resonance mode distribution,[18,22,47] they typically require expensive and time-consuming processes of design optimization and remanufacturing. In contrast, our proposed NCAA accomplishes this goal through a programmable digital

transition from impedance matching to mismatching at the absorber interface, as depicted in Figures 4E and 4F. With the active nature of our absorber, it is possible to achieve a negative acoustic resistance, thereby enabling a reflection coefficient greater than 1 in the stopband. This expanded modulation range of the reflection coefficient surpasses its passive counterparts. These examples illustrate the capability of the NCAA to achieve an adjustable absorption spectrum. In principle, other diverse absorption spectra can also be synthesized by simply modifying the shaping filter $f(n)$, opening possibilities for the exploration of additional practical operations.

DISCUSSION

In this work, we presented an NCAA that surpasses the causality limit by relying on a feedforward mechanism to provide *a priori* information to the absorber on the incoming signal. This approach enables the minimization of the footprint of absorbers while preserving a broad bandwidth of operation. While conventional active approaches in metamaterials commonly incur in instabilities,[49] our approach avoids stability issues. The demonstrated strategy for broadband absorption can be extended to other wave platforms, including waves for which the propagation speed of the background medium is fast. Although the active absorber shown here operates in a one-dimensional waveguide, it is possible to increase its effective area by combining multiple units into a surface array, as in the case of metasurfaces.[50–52]

While only normal incidence was considered in this work, oblique incidence and complex wavefronts may also be addressed with an extended model, following similar constraints. The active absorber was designed here to obtain efficient absorption performance beyond the causality limit within a low profile, different from tube noise-canceling systems[53] and noise-canceling earplugs,[54] which primarily focus on sound cancellation through interference to prevent noise transmission. We emphasize that our *a priori* signals are only used to carry noncausal information to the absorber to modify its response in time, which is less energy demanding compared to approaches that leverage destructive interference, as in noise cancellation. Furthermore, aiming to challenge the causality limit, our device was designed to support a thin form factor, which is different from previously proposed hybrid active-passive absorbers that tend to be significantly thicker.[55,56] The weight of the proposed active absorber is mainly due to the presence of the loudspeaker, which can be reduced by choosing lighter-weight models in practical applications. This proposed design strategy holds promise in architectural acoustics, selective sound communications, and broadband noise mitigation. A known noise signal was used as a proof-of-concept demonstration, which has been a common practice for active absorbers.[57,58] Nevertheless, leveraging a feedback neutralization technique,[59] our absorber can still achieve sound absorption by sampling the incoming signals to leverage *a priori* information (see Note S6 and Figure S3).

In summary, we presented a comprehensive analysis of the impact of causality on sound absorption in materials. We have shown that the causality limit of absorbers can be overcome by adopting an active approach that breaks the causality of the system. A theoretical framework is established between the minimum dimension of absorbers and the degree of causality violation, which sets the physical bounds for NCAAs. The results are verified by measurements based on an active absorber that harnesses noncausal information. Over 90% sound absorption was experimentally demonstrated within the 150–1,600 Hz frequency range with a thickness of only 82.5 mm, far thinner than the equivalent minimum thickness of 374.3 mm dictated by the causal limit. Our result highlights the effectiveness of NCAA in reducing the thickness of sound absorbers, which is of great importance for broadband noise mitigation. By adjusting the time delay in the system, we showed the minimum thickness dependence on the degree of causality breaking. Furthermore, we demonstrated the flexibility of our approach by programming the controller to achieve adjustable absorption spectra without the need for structural modifications. This feature offers great convenience in practical applications and represents a step forward to realize user-desired, in-demand sound scattering beyond causal limits.

Although near-perfect broadband absorption was only demonstrated for the 150–1,600 Hz range, the operating frequency band of the noncausal absorber can be adjusted by using corresponding noise source signals to train the controller for noise sources at various frequencies. Moreover, the efficient bandwidth of the active absorber can be improved by using a high-performance controller. The obtained results demonstrate the efficacy of an active structural design in reducing the size of acoustic absorbers and shed light on the influence of causality in sound absorption. This concept holds promise for various applications involving wave modulation, including absorber designs,[60,61] acoustic stealth cloaks,[62,63] and acoustic Willis coupling metamaterials,[64–66] offering opportunities to realize broadband resonant responses that go beyond the stringent bandwidth limitations introduced by causality.

EXPERIMENTAL PROCEDURES

Resource availability

Lead contact
Further information and requests for resources should be directed to and will be fulfilled by the lead contact, Andrea Alù (aalu@gc.cuny.edu).

Materials availability
This study did not generate new unique reagents.

Data and code availability
The data that support the findings of this study are available within the paper and its supplemental information files. Additional data and files are available from the corresponding author upon reasonable request.

Experimental measurements
The experimental setup is depicted in Figure 2B. Two HiviB4N loudspeakers are used to constitute the noise source and the active absorber, respectively. A multichannel analyzer (B&K PULSE 3160A) is used to generate noise signal. The absorption coefficient is measured using the transfer function method, employing two 1/2-inch microphones labeled as A and B. These microphones are positioned 8 cm apart, with microphone B located at a distance of 50 cm from the absorber interface S. Calibration procedures are conducted to improve amplitude and phase agreement between the two microphones, which is important to obtain accurate measurement results.

REFERENCES

1. Milton, G.W., Eyre, D.J., and Mantese, J.V. (1997). Finite frequency range Kramers Kronig relations: Bounds on the dispersion. Phys. Rev. Lett. *79*, 3062–3065. https://doi.org/10.1103/PhysRevLett.79.3062.

2. Waters, K.R., Mobley, J., and Miller, J.G. (2005). Causality-imposed (Kramers-Kronig) relationships between attenuation and dispersion. IEEE Trans. Ultrason. Ferroelectr. Freq. Control *52*, 822–833. https://doi.org/10.1109/tuffc.2005.1503968.

3. Chu, L.J. (1948). Physical Limitations of Omni-Directional Antennas. J. Appl. Phys. *19*, 1163–1175. https://doi.org/10.1063/1.1715038.

4. McLean, J.S. (1996). A re-examination of the fundamental limits on the radiation Q of electrically small antennas. IEEE Trans. Antennas Propag. *44*, 672–676. https://doi.org/10.1109/8.496253.

5. Sievenpiper, D.F., Dawson, D.C., Jacob, M.M., Kanar, T., Kim, S., Long, J., and Quarfoth, R.G. (2012). Experimental Validation of Performance Limits and Design Guidelines for Small Antennas. IEEE Trans. Antennas Propag. *60*, 8–19. https://doi.org/10.1109/tap.2011.2167938.

6. Rasmussen, C., and Alu, A. (2021). Non-Foster acoustic radiation from an active piezoelectric transducer. Proc. Natl. Acad. Sci. USA *118*, e2024984118. https://doi.org/10.1073/pnas.2024984118.

7. Bode, H.W. (1945). Network analysis and feedback amplifier design (Van Nostrand).

8. Fano, R.M. (1950). Theoretical limitations on the broadband matching of arbitrary impedances. J. Franklin Inst. *249*, 57–83. https://doi.org/10.1016/0016-0032(50)90006-8.

9. Li, H., Mekawy, A., and Alu, A. (2019). Beyond Chu's limit with Floquet impedance matching. Phys. Rev. Lett. *123*, 164102. https://doi.org/10.1103/PhysRevLett.123.164102.

10. Monticone, F., and Alù, A. (2013). Do cloaked objects really scatter less? Phys. Rev. X *3*, 041005. https://doi.org/10.1103/PhysRevX.3.041005.

11. Fleury, R., Monticone, F., and Alu, A. (2015). Invisibility and cloaking: origins, present, and future perspectives. Phys. Rev. Appl. *4*, 037001. https://doi.org/10.1103/PhysRevApplied.4.037001.

12. Norris, A.N. (2015). Acoustic integrated extinction. Proc. R. Soc. A *471*, 20150008. https://doi.org/10.1098/rspa.2015.0008.

13. Monticone, F., and Alu, A. (2016). Invisibility exposed: physical bounds on passive cloaking. Optica *3*, 718–724. https://doi.org/10.1364/Optica.3.000718.

14. Muhlestein, M.B., Sieck, C.F., Alu, A., and Haberman, M.R. (2016). Reciprocity, passivity and causality in Willis materials. Proc. R. Soc. A *472*, 20160604. https://doi.org/10.1098/rspa.2016.0604.

15. Quan, L., Yves, S., Peng, Y., Esfahlani, H., and Alu, A. (2021). Odd Willis coupling induced by broken time-reversal symmetry. Nat. Commun. *12*, 2615. https://doi.org/10.1038/s41467-021-22745-5.

16. Rozanov, K.N. (2000). Ultimate thickness to bandwidth ratio of radar absorbers. IEEE Trans. Antennas Propag. *48*, 1230–1234. https://doi.org/10.1109/8.884491.

17. Acher, O., Bernard, J.M., Marechal, P., Bardaine, A., and Levassort, F. (2009). Fundamental constraints on the performance of broadband ultrasonic matching structures and absorbers. J. Acoust. Soc. Am. *125*, 1995–2005. https://doi.org/10.1121/1.3081529.

18. Yang, M., Chen, S.Y., Fuab, C.X., and Sheng, P. (2017). Optimal sound-absorbing structures. Mater. Horiz. *4*, 673–680. https://doi.org/10.1039/c7mh00129k.

19. Ma, G., Yang, M., Xiao, S., Yang, Z., and Sheng, P. (2014). Acoustic metasurface with hybrid resonances. Nat. Mater. *13*, 873–878. https://doi.org/10.1038/nmat3994.

20. Li, Y., and Assouar, B.M. (2016). Acoustic metasurface-based perfect absorber with deep subwavelength thickness. Appl. Phys. Lett. *108*, 063502. https://doi.org/10.1063/1.4941338.

21. Aurégan, Y. (2018). Ultra-thin low frequency perfect sound absorber with high ratio of active area. Appl. Phys. Lett. *113*, 201904. https://doi.org/10.1063/1.5063504.

22. Zhou, Z., Huang, S., Li, D., Zhu, J., and Li, Y. (2022). Broadband impedance modulation via non-local acoustic metamaterials. Natl. Sci. Rev. *9*, nwab171. https://doi.org/10.1093/nsr/nwab171.

23. Qu, S., Hou, Y., and Sheng, P. (2021). Conceptual-based design of an ultrabroadband microwave metamaterial absorber. Proc. Natl. Acad. Sci. USA *118*, e2110490118. https://doi.org/10.1073/pnas.2110490118.

24. Qu, S., Gao, N., Tinel, A., Morvan, B., Romero-Garcia, V., Groby, J.P., and Sheng, P. (2022). Underwater metamaterial absorber with impedance-matched composite. Sci. Adv. *8*, eabm4206. https://doi.org/10.1126/sciadv.abm4206.

25. Mak, H.Y., Zhang, X.N., Dong, Z., Miura, S., Iwata, T., and Sheng, P. (2021). Going beyond the causal limit in acoustic absorption. Phys. Rev. Appl. *16*, 044062. https://doi.org/10.1103/PhysRevApplied.16.044062.

26. Shaltout, A.M., Shalaev, V.M., and Brongersma, M.L. (2019). Spatiotemporal light control with active metasurfaces. Science *364*, eaat3100. https://doi.org/10.1126/science.aat3100.

27. Shlivinski, A., and Hadad, Y. (2018). Beyond the Bode-Fano bound: wideband impedance matching for short pulses using temporal switching of transmission-line parameters. Phys. Rev. Lett. *121*, 204301. https://doi.org/10.1103/PhysRevLett.121.204301.

28. Li, H., Yin, S., and Alu, A. (2022). Nonreciprocity and Faraday rotation at time interfaces. Phys. Rev. Lett. *128*, 173901. https://doi.org/10.1103/PhysRevLett.128.173901.

29. Rizza, C., Castaldi, G., and Galdi, V. (2022). Short-pulsed metamaterials. Phys. Rev. Lett. *128*, 257402. https://doi.org/10.1103/PhysRevLett.128.257402.

30. Li, H., and Alù, A. (2020). Temporal switching to extend the bandwidth of thin absorbers. Optica *8*, 24–29. https://doi.org/10.1364/optica.408399.

31. Hayran, Z., Chen, A.B., and Monticone, F. (2021). Spectral causality and the scattering of waves. Optica *8*, 1040–1049. https://doi.org/10.1364/Optica.423089.

32. Firestein, C., Shlivinski, A., and Hadad, Y. (2022). Absorption and scattering by a temporally switched lossy layer: going beyond the Rozanov bound. Phys. Rev. Appl. *17*, 014017. https://doi.org/10.1103/PhysRevApplied.17.014017.

33. Yang, X.Z., Wen, E., and Sievenpiper, D.F. (2022). Broadband time-modulated absorber beyond the Bode-Fano limit for short pulses by energy trapping. Phys. Rev. Appl. *17*, 044003. https://doi.org/10.1103/PhysRevApplied.17.044003.

34. Cummer, S.A., Christensen, J., and Alù, A. (2016). Controlling sound with acoustic metamaterials. Nat. Rev. Mater. *1*, 16001. https://doi.org/10.1038/natrevmats.2016.1.

35. Fleury, R., Sounas, D., and Alu, A. (2015). An invisible acoustic sensor based on parity-time symmetry. Nat. Commun. *6*, 5905. https://doi.org/10.1038/ncomms6905.

36. Shi, C., Dubois, M., Chen, Y., Cheng, L., Ramezani, H., Wang, Y., and Zhang, X. (2016). Accessing the exceptional points of parity-time symmetric acoustics. Nat. Commun. *7*, 11110. https://doi.org/10.1038/ncomms11110.

37. Popa, B.I., and Cummer, S.A. (2014). Non-reciprocal and highly nonlinear active acoustic metamaterials. Nat. Commun. *5*, 3398. https://doi.org/10.1038/ncomms4398.

38. Cho, C., Wen, X., Park, N., and Li, J. (2020). Digitally virtualized atoms for acoustic metamaterials. Nat. Commun. *11*, 251. https://doi.org/10.1038/s41467-019-14124-y.

39. Chen, P.Y., Argyropoulos, C., and Alu, A. (2013). Broadening the cloaking bandwidth with non-Foster metasurfaces. Phys. Rev. Lett. *111*, 233001. https://doi.org/10.1103/PhysRevLett.111.233001.

40. Mou, J.C., and Shen, Z.X. (2017). Design and experimental demonstration of non-Foster active absorber. IEEE Trans. Antennas Propag. *65*, 696–704. https://doi.org/10.1109/Tap.2016.2639012.

41. Srivastava, A. (2021). Causality and passivity: From electromagnetism and network theory to metamaterials. Mech. Mater. *154*, 103710. https://doi.org/10.1016/j.mechmat.2020.103710.

42. Cao, L.T., Fu, Q.X., Si, Y., Ding, B., and Yu, J.Y. (2018). Porous materials for sound absorption. Compos. Commun. *10*, 25–35. https://doi.org/10.1016/j.coco.2018.05.001.

43. Xiao, T., Qiu, X., and Halkon, B. (2020). Ultra-broadband local active noise control with remote acoustic sensing. Sci. Rep. *10*, 20784. https://doi.org/10.1038/s41598-020-77614-w.

44. Xiao, T., Halkon, B., Wang, S., Oberst, S., and Qiu, X. (2024). Refracto-vibrometry for active control of sound radiation through an opening. J. Sound Vib. *577*, 118242. https://doi.org/10.1016/j.jsv.2024.118242.

45. Popa, B.I., and Cummer, S.A. (2009). Design and characterization of broadband acoustic composite metamaterials. Phys. Rev. B *80*, 174303. https://doi.org/10.1103/PhysRevB.80.174303.

46. Elliott, S. (2001). Signal Processing for Active Control (Academic Press), pp. 142–143.

47. Shao, C., Zhu, Y.Z., Long, H.Y., Liu, C., Cheng, Y., and Liu, X.J. (2022). Metasurface absorber for ultra-broadband sound via over-damped modes coupling. Appl. Phys. Lett. *120*, 083504. https://doi.org/10.1063/5.0080930.

48. Kuo, S.M., and Tsai, J.M. (1994). Residual noise shaping technique for active noise-control systems. J. Acoust. Soc. Am. *95*, 1665–1668. https://doi.org/10.1121/1.408555.

49. Duggan, R., Moussa, H., Ra'di, Y., Sounas, D.L., and Alù, A. (2022). Stability bounds on superluminal propagation in active structures. Nat. Commun. *13*, 1115. https://doi.org/10.1038/s41467-022-28713-x.

50. Bok, E., Park, J.J., Choi, H., Han, C.K., Wright, O.B., and Lee, S.H. (2018). Metasurface for water-to-air sound transmission. Phys. Rev. Lett. *120*, 044302. https://doi.org/10.1103/PhysRevLett.120.044302.

51. Ma, G., Fan, X., Sheng, P., and Fink, M. (2018). Shaping reverberating sound fields with an actively tunable metasurface. Proc. Natl. Acad. Sci. USA *115*, 6638–6643. https://doi.org/10.1073/pnas.1801175115.

52. Popa, B.I., Zhai, Y., and Kwon, H.S. (2018). Broadband sound barriers with bianisotropic metasurfaces. Nat. Commun. *9*, 5299. https://doi.org/10.1038/s41467-018-07809-3.

53. Wu, L.F., Qiu, X.J., and Guo, Y.C. (2014). A simplified adaptive feedback active noise control system. Appl. Acoust. *81*, 40–46. https://doi.org/10.1016/j.apacoust.2014.02.006.

54. Zhang, L.M., and Qju, X.J. (2014). Causality study on a feedforward active noise control headset with different noise coming directions in free field. Appl. Acoust. *80*, 36–44. https://doi.org/10.1016/j.apacoust.2014.01.004.

55. Cobo, P., Fernandez, A., and Doutres, O. (2003). Low-frequency absorption using a two-layer system with active control of input impedance. J. Acoust. Soc. Am. *114*, 3211–3216. https://doi.org/10.1121/1.1629306.

56. Cobo, P., and Cuesta, M. (2009). Measuring hybrid passive-active sound absorption of a microperforated liner at oblique incidence. J. Acoust. Soc. Am. *125*, 185–190. https://doi.org/10.1121/1.3026328.

57. Ma, X.Y., Yurchenko, D., Chen, K., Wang, L., Liu, Y., and Yang, K. (2022). Structural acoustic controlled active micro-perforated panel absorber for improving wide-band low frequency sound absorption. Mech. Syst. Signal Process. *178*, 109295. https://doi.org/10.1016/j.ymssp.2022.109295.

58. An, F., Zhao, P., Li, X., Wu, Q., and Liu, B. (2024). Active impedance control of a loudspeaker and its parallel combination with porous materials for broadband sound absorption. Mech. Syst. Signal Process. *206*, 110909. https://doi.org/10.1016/j.ymssp.2023.110909.

59. Kuo, S.M., and Morgan, D.R. (1996). Active Noise Control Systems (Wiley), pp. 82–85.

60. Li, X.P., Chen, Y.Y., Zhu, R., and Huang, G.L. (2021). An active meta-layer for optimal flexural wave absorption and cloaking. Mech. Syst. Signal Process. *149*, 107324. https://doi.org/10.1016/j.ymssp.2020.107324.

61. Cao, L., Zhu, Y., Wan, S., Zeng, Y., and Assouar, B. (2022). On the design of non-Hermitian elastic metamaterial for broadband perfect absorbers. Int. J. Eng. Sci. *181*, 103768. https://doi.org/10.1016/j.ijengsci.2022.103768.

62. Popa, B.-I., Zigoneanu, L., and Cummer, S.A. (2011). Experimental acoustic ground cloak in air. Phys. Rev. Lett. *106*, 253901. https://doi.org/10.1103/PhysRevLett.106.253901.

63. Zigoneanu, L., Popa, B.-I., and Cummer, S.A. (2014). Three-dimensional broadband omnidirectional acoustic ground cloak. Nat. Mater. *13*, 352–355. https://doi.org/10.1038/nmat3901.

64. Koo, S., Cho, C., Jeong, J.H., and Park, N. (2016). Acoustic omni meta-atom for decoupled access to all octants of a wave parameter space. Nat. Commun. *7*, 13012. https://doi.org/10.1038/ncomms13012.

65. Muhlestein, M.B., Sieck, C.F., Wilson, P.S., and Haberman, M.R. (2017). Experimental evidence of Willis coupling in a one-dimensional effective material element. Nat. Commun. *8*, 15625. https://doi.org/10.1038/ncomms15625.

66. Sieck, C.F., Alù, A., and Haberman, M.R. (2017). Origins of Willis coupling and acoustic bianisotropy in acoustic metamaterials through source-driven homogenization. Phys. Rev. B *96*, 104303. https://doi.org/10.1103/PhysRevB.96.104303.